Centrality dependence of the pseudorapidity density distribution for charged particles in Pb–Pb collisions at √sNN = 2.76 TeV

(ALICE Collaboration) Abelev, B.; ...; Antičić, Tome; ...; Gotovac, Sven; ...; Mudnić, Eugen; ...; Planinić, Mirko; ...; ...

Source / Izvornik: **Physics Letters B, 2013, 726, 610 - 622**

Journal article, Published version
Rad u časopisu, Objavljena verzija rada (izdavačev PDF)

https://doi.org/10.1016/j.physletb.2013.09.022

Permanent link / Trajna poveznica: https://urn.nsk.hr/urn:nbn:hr:217:872483

Physics Letters B 726 (2013) 610–622

Contents lists available at ScienceDirect

Physics Letters B

www.elsevier.com/locate/physletb

Centrality dependence of the pseudorapidity density distribution for charged particles in Pb–Pb collisions at $\sqrt{s_{\mathrm{NN}}} = 2.76$ TeV ☆

ALICE Collaboration

ARTICLE INFO

Article history:
Received 12 April 2013
Received in revised form 27 July 2013
Accepted 12 September 2013
Available online 18 September 2013
Editor: L. Rolandi

Keywords:
LHC
Heavy-ion collisions
Charged-particle density
Wide rapidity coverage

ABSTRACT

We present the first wide-range measurement of the charged-particle pseudorapidity density distribution, for different centralities (the 0–5%, 5–10%, 10–20%, and 20–30% most central events) in Pb–Pb collisions at $\sqrt{s_{\mathrm{NN}}} = 2.76$ TeV at the LHC. The measurement is performed using the full coverage of the ALICE detectors, $-5.0 < \eta < 5.5$, and employing a special analysis technique based on collisions arising from LHC 'satellite' bunches. We present the pseudorapidity density as a function of the number of participating nucleons as well as an extrapolation to the total number of produced charged particles ($N_{\mathrm{ch}} = 17\,165 \pm 772$ for the 0–5% most central collisions). From the measured $\mathrm{d}N_{\mathrm{ch}}/\mathrm{d}\eta$ distribution we derive the rapidity density distribution, $\mathrm{d}N_{\mathrm{ch}}/\mathrm{d}y$, under simple assumptions. The rapidity density distribution is found to be significantly wider than the predictions of the Landau model. We assess the validity of longitudinal scaling by comparing to lower energy results from RHIC. Finally the mechanisms of the underlying particle production are discussed based on a comparison with various theoretical models.

1. Introduction

There exists much evidence that, under the extreme conditions of unprecedented temperature and energy density created in ultra-relativistic heavy-ion collisions, matter is in a deconfined state known as the quark–gluon plasma [1–4]. A new era in the study of these collisions began with the production of Pb–Pb collisions at a center-of-mass energy per nucleon pair $\sqrt{s_{\mathrm{NN}}} = 2.76$ TeV at the CERN LHC.

The charged-particle pseudorapidity density generated in heavy-ion collisions depends on the particle production mechanisms as well as on the initial energy density. Studying the dependence of the pseudorapidity density on collision centrality will improve our understanding of the role of hard scattering and soft processes contributing to the production of charged particles (e.g. parton saturation [5]). Moreover, extending the measurement to a wide pseudorapidity range enables investigating the physics of the fragmentation region by comparing the extrapolation of this data to lower energy data from RHIC [6,7] to test whether longitudinal scaling of the pseudorapidity density persists up to LHC energies.

In this Letter we present the first LHC measurement over a wide pseudorapidity range of the centrality dependence of the charged-particle pseudorapidity density, $\mathrm{d}N_{\mathrm{ch}}/\mathrm{d}\eta$, utilizing the ALICE detector. The employed method relies on using so-called 'satellite' bunch collisions and is based on measurements from three different ALICE sub-detectors. This method is applicable for the 30% most central events where the trigger efficiency for these 'satellite' collisions remains high. These measurements extend considerably the former results obtained at the LHC [8–10] and can be compared to the wealth of results on the charged-particle pseudorapidity density from lower energy Au–Au collisions at RHIC [6,11,12] as well as model calculations.

2. Experimental setup

A detailed description of the ALICE detector can be found in [13]. In the following, we will briefly describe the detectors used in this analysis, namely the Silicon Pixel Detector (SPD), the Forward Multiplicity Detector (FMD), the VZERO, and the Zero Degree Calorimeter (ZDC) (see Fig. 1).

The SPD is the innermost element of the ALICE inner tracking system [13]. It consists of two cylindrical layers of hybrid silicon pixel assemblies positioned at radial distances of 3.9 and 7.6 cm from the beam line, with a total of 9.8×10^6 pixels of size 50×425 μm^2, read out by 1200 electronic chips. The SPD coverage for particles originating from the nominal interaction point at the center of the detector is $|\eta| < 2$ and $|\eta| < 1.4$ for the inner and outer layers, respectively.

The VZERO detector [14] consists of two arrays of 32 scintillator tiles (4 rings of increasing radii each with 8 azimuthal sectors) placed at distances of 3.3 m (VZERO-A) and −0.9 m (VZERO-C) from the nominal interaction point along the beam axis, covering the full azimuth within $2.8 < \eta < 5.1$ and $-3.7 < \eta < -1.7$,

☆ © CERN for the benefit of the ALICE Collaboration.

0370-2693/
http://dx.doi.org/10.1016/j.physletb.2013.09.022

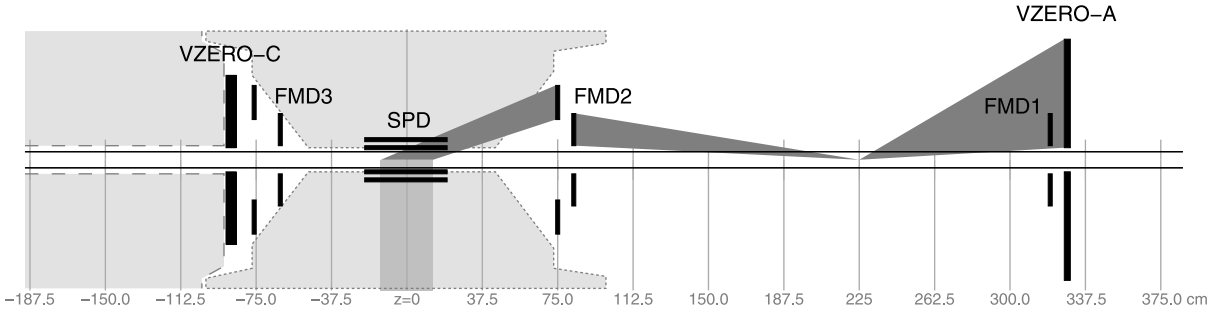

Fig. 1. Schematic drawing (not to scale) of the cross-section of the sub-detectors used in this analysis and the midpoints of the locations of the nominal and 'satellite' interaction points. The long-dashed line designates a region of dense material designed to absorb all particles except muons. The short-dashed line indicates the region of the ALICE inner tracking system, which has dense material for its services on the surfaces near FMD2 and FMD3. The area between FMD2, FMD1 and VZERO-A contains only the beryllium beam pipe. The dark gray shaded areas denote the paths particles would follow from $z = 0$ cm and $z = 225$ cm to FMD2 and VZERO-A such that it is evident which material they would traverse.

respectively. Both the amplitude and the time of the signal in each scintillator are recorded.

The ZDC measures the energy of spectator (non-interacting) nucleons in two identical sets of detectors, located at ± 114 m from the interaction point along the beam axis [13]. Each set consists of two quartz fiber sampling calorimeters: a neutron calorimeter positioned between the two LHC beam pipes down-stream of the first LHC dipole which separates the two charged-particle beams and a proton calorimeter positioned externally to the beam pipe containing bunches moving away from the interaction point. The ZDC energy resolution at the Pb beam energy is estimated to be 20% and 25% for the neutron and proton calorimeters, respectively. The ZDC system is completed by two Zero-degree Electro-Magnetic (ZEM) calorimeters placed at $+7.5$ m from the interaction point along the beam direction [13]. They cover the pseudorapidity range between 4.8 and 5.7 and thus measure the energy of particles emitted at very small angles with respect to the beam axis.

The FMD [15] is composed of three sub-detectors: FMD1, FMD2, and FMD3. FMD2 and FMD3 consist of an inner and an outer ring of silicon strip sensors, while FMD1 consists of only an inner ring. The inner and outer rings have internal radii of 4.2 cm and 15.4 cm and external radii of 17.2 cm and 28.4 cm, respectively, with full azimuthal coverage. Each ring is sub-divided into 512 or 256 radial strips and 20 or 40 azimuthal sectors for inner and outer rings, respectively. For collisions at the nominal interaction point the pseudorapidity coverage is $-3.4 < \eta < -1.7$ (FMD3) and $1.7 < \eta < 5.0$ (FMD2 and FMD1). Each sub-ring has 10 240 channels resulting in a total of 51 200 channels.

3. Data sample and analysis approach

The analysis presented in this Letter is based on Pb–Pb collision data at $\sqrt{s_{\mathrm{NN}}} = 2.76$ TeV taken by ALICE in 2010.

Results in the region of $|\eta| < 2$ are obtained from a tracklet analysis using the two layers of the SPD. The analysis method and the used data sample are identical to the ones described in [16], but extending the pseudorapidity range of the SPD detector by using collisions occurring within ± 13 cm (rather than ± 10 cm) from the nominal interaction point along the beam axis.

The measurement of multiplicity in the region $|\eta| > 2$ is carried out using the FMD and VZERO. The main challenge in the analysis of these data is the correction for secondary particles produced by primary particles interacting with the detector material. While the low material density in the ALICE central barrel limits the number of secondary particles, for $|\eta| > 2$ dense material – such as services, cooling tubes, and read-out cables – is present. This material causes a very large production of secondary particles, in some cases up to twice the number of primary particles as obtained from Monte Carlo studies. Furthermore, the geometry and segmentation of the two detectors do not allow for the rejection of secondary particles through tracklet reconstruction and therefore the analysis depends strongly on Monte Carlo driven corrections. In order to reduce systematic effects arising from these large correction factors, a special analysis technique was developed. It relies on the so-called 'debunching' effect which occurs during the injection and acceleration of the beams inside the LHC ring [17]. Due to the way the beams are injected and transferred to the LHC, a small fraction of the beam can be captured in unwanted RF buckets which creates so-called 'satellite' bunches spaced by 2.5 ns. Thus crossings of the 'satellite' bunches of one beam with the main bunches of the opposite beam produce 'satellite' interactions with vertices spaced by 37.5 cm in the longitudinal direction (see Fig. 1). These interactions provide the opportunity to avoid the large amount of material traversed by particles coming from the nominal vertex and to extend the pseudorapidity range of the FMD and VZERO. Interactions with vertices from -187.5 cm to 375 cm are used in this analysis. Furthermore, FMD3 and VZERO-C are surrounded by dense material and, therefore, only the FMD1, FMD2, and VZERO-A were used. For 'satellite' collisions in the range of $75, 102.5, \ldots, 300$ cm from the nominal interaction point along the beam axis, the only material between the VZERO-A, FMD1, FMD2 and the interaction point is the beryllium beam pipe, resulting in a reduction of the number of secondary particles by more than a factor of two in Monte Carlo simulations and consequently much smaller corrections. For vertices with $z > 300$ cm and $z < 75$ cm other detector material has an increasing influence on the measurement such that for vertices with $z < 37.5$ cm only FMD1 and the inner ring of VZERO-A are used. An additional advantage of this analysis method is the possibility for a data-driven calibration of the detector response using 'satellite' collisions for which the pseudorapidity coverage of the VZERO overlaps with the nominal SPD acceptance, as it will be explained in the following.

Due to the fact that the 'satellite' collision vertices fall outside the normal range around the nominal interaction point, the standard ALICE trigger and event selection [8] is inapplicable. Therefore a special trigger imposing a lower cut of 100 fired chips on both layers of the SPD was used. The trigger was verified to be fully efficient for the centrality range covered by the present analysis. This was done by inspecting the distribution of the number of fired SPD chips as a function of the event centrality. The triggered events are then further selected based on the ZDC timing information, so that

$$\frac{(\Delta T - n \times 2.5\ \mathrm{ns})^2}{(\sigma_{\Delta T})^2} + \frac{(\Sigma T - n \times 2.5\ \mathrm{ns})^2}{(\sigma_{\Sigma T})^2} < 1,$$

where ΔT and ΣT are the difference and sum of the arrival times (relative to the crossing time of the main bunches) of the signals in the two ZDC calorimeters, respectively, and $\sigma_{\Delta T} = 1.32$ ns and $\sigma_{\Sigma T} = 2.45$ ns are the corresponding resolutions. n is the index of the 'satellite' interaction point, such that $n = 0$ denotes an interaction at the nominal interaction point. More details on the event selection can be found in [18]. It is worth noting that the crossing angle between the beams was zero during the Pb–Pb data taking in 2010 which naturally enriched the data sample with 'satellite' collisions. The rate of the 'satellite' collisions is about three orders of magnitude lower than the rate of the nominal collisions and therefore, in order to accumulate a sufficient amount of events, the analysis was performed with all 'satellite' collisions from the entire 2010 data sample. The acquired statistics is distributed unevenly among the different 'satellite' vertices and varies from one thousand to twelve thousand events per vertex.

Similarly to the trigger and event selection, the standard centrality selection based on VZERO [18] cannot be used in the analysis of the 'satellite' collisions. Given the fact that the ZDC and ZEM are positioned very far away from the nominal interaction point, they are best suited for the characterization of 'satellite' collisions. The event sample is split into four centrality classes (0–5%, 5–10%, 10–20%, and 20–30%) based on the energy deposited by spectator nucleons in the ZDC and by particles emitted at small angles with respect to the beam axis in the ZEM. The number of spectator nucleons and, therefore, their deposited energy decreases for more central events while the inverse is true for particles emitted at small angles with respect to the beam axis. One can therefore define centrality cuts based on this anti-correlation. In order to match this estimator to the standard ALICE centrality selection, the correlation between the ZDC versus ZEM and VZERO signal for events near the nominal interaction point is determined [18]. This method is only reliable in the centrality range 0–30% where the trigger is also fully efficient; this defines the centrality range for the presented measurement. To reduce the residual bias arising from the position of the interaction point, the ZEM signal is scaled as a function of 'satellite' vertex. The scaling factors are obtained by a linear fit to the ZDC versus ZEM anti-correlation. They are found to be between 0.96 and 1.04 for vertices from −187.5 cm to 225 cm and about 0.86 for the farthest vertex at 375 cm.

The FMD and VZERO are used to extract the multiplicity independently in the same η acceptance. The FMD records the energy loss of particles that traverse each silicon strip. The first step in the analysis is to apply a minimum cut on the measured energy to neglect strips considered to have only electronics noise. Due to the incident angle of the particles impinging on the detector, the energy loss signal of one particle may be spread out over more than one strip. The next step in the analysis is therefore to cluster individual strip signals corresponding to the energy of a single particle. This is accomplished by adding the strip signals which are below a clustering threshold to neighboring strips which have a larger signal if one exists. The finite resolution of the FMD also allows for more than one particle to traverse a single strip. The number of charged particles per strip is then determined using a statistical approach where the mean number of particles per strip, μ, over a region of 256 strips (64 strips radially × 4 strips azimuthally) is estimated assuming a Poisson distribution, such that $\mu = -\ln(N_E/N_S)$, where N_E is the number of strips with no hits and N_S is the total number of strips (256 here) in the defined region. To get the average number of particles per hit strip, a correction of $c = \frac{\mu}{1-e^{-\mu}}$ is applied to each hit strip in the region. Next, the data are corrected for the acceptance at a given interaction point, and the inclusive charged-particle count is converted to the number of primary charged particles by means of an interaction-point and centrality-dependent response map. These response maps are based on GEANT3 [19] Monte Carlo simulations using the HIJING event generator [20] and relate the number of generated primary charged particles in a given (η, φ) bin (bins are of size 0.05 in η and $\pi/10$ in φ) to the total number of charged particles reduced by the detector efficiency in the same bin. The response maps are highly sensitive to the accuracy of the experimental description in the simulation, and are therefore the largest source of the systematic error on the results from the FMD.

Table 1
List of the considered systematic errors.

Detector	Source	Error
Common	Centrality	1–2%
SPD	Background subtraction	0.1–2%
	Particle composition	1%
	Weak decays	1%
	Extrapolation to zero momentum	2%
FMD & VZERO	Material budget	4%
	ZEM scaling	1–4%
FMD	Particle composition, spectra, weak decays	2%
	Variation of cuts	3%
	Analysis method	2%
VZERO	Variation between rings	3%
	Calibration by SPD	3–4%

In order to calculate the charged-particle density in the VZERO detector, the Monte Carlo simulation described above is used to relate the observed signal to the number of primary charged particles within the acceptance of a given VZERO ring. The relation is given by $A(z,i) = \alpha(z,i) N_{ch}(\eta(z,i))$, where i is the ring index and z is the longitudinal position of the interaction point. A is the VZERO signal amplitude, N_{ch} is the number of primary charged particles in the VZERO ring's acceptance from the given interaction point, and α is the conversion factor between A and N_{ch} determined from the Monte Carlo simulation. In order to minimize the dependence on the simulation and perform a data-driven analysis, the VZERO response is calibrated using reference 'satellite' vertices, z_r, between 225 cm and 375 cm for which the pseudorapidity coverage of the VZERO rings lies inside $|\eta| < 2$, i.e. overlapping the range of the SPD at the nominal interaction point. In this way the charged-particle pseudorapidity density in a given ring of the VZERO detector and for a given interaction point, in the range of -187.5 cm $\leqslant z \leqslant 375$ cm, is obtained as:

$$\frac{dN_{ch}^{VZERO}}{d\eta}\big(\eta(z,i)\big) = \frac{dN_{ch}^{SPD}}{d\eta}\big(\eta(z_r,i)\big)\frac{\alpha(z_r,i)}{\alpha(z,i)}\frac{A(z,i)}{A(z_r,i)},$$

where $dN_{ch}^{SPD}/d\eta$ is the charged-particle pseudorapidity density measured by the SPD, z_r is the longitudinal position of the reference vertex and η is the pseudorapidity corresponding to the chosen vertex and VZERO ring. The factors α represent the full detector response including secondary particles, light yield per particle, and electronics response of the VZERO, and are checked to be constant for the selected range of 'satellite' vertices.

Finally, a small correction (up to 1%) is applied to the VZERO data points arising from a residual bias in the method determined from Monte Carlo simulations by comparing the final reconstructed $dN_{ch}/d\eta$ distribution after combining the results from all vertices to the Monte Carlo input $dN_{ch}/d\eta$ distribution.

4. Systematic errors

Table 1 summarizes the various contributions to the systematic errors for each of the three detectors used, as well as the common contribution arising from the uncertainty in the centrality determination. The latter is assessed by comparing the SPD results

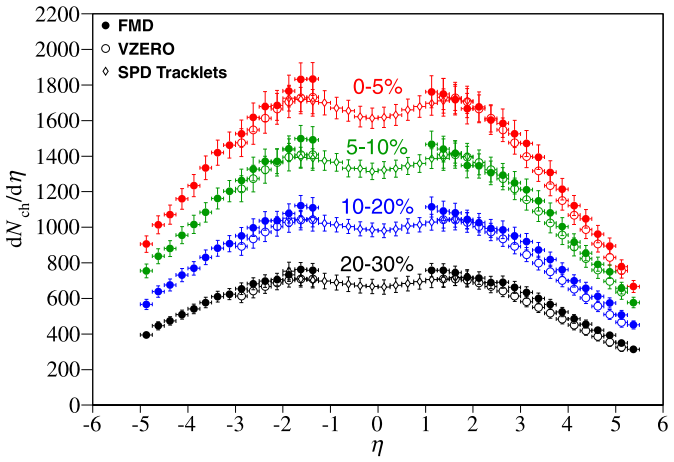

Fig. 2. $dN_{ch}/d\eta$ per centrality bin from each of the three detectors used. The error bars correspond to the total statistical and systematic error.

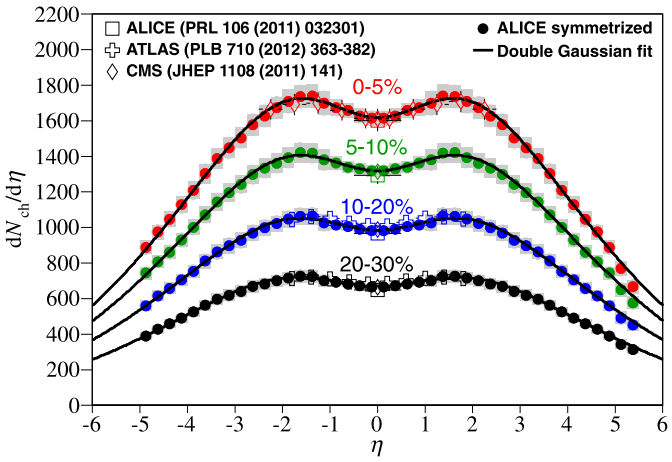

Fig. 3. Combined $dN_{ch}/d\eta$ result per centrality bin. The error bars (gray boxes) show the total statistical and systematic error of the combined result. The open squares indicate the previously published ALICE result near mid-rapidity [16]. Published results from other LHC experiments [9,10] which have the same centrality as the ALICE measurement are also shown.

obtained with the standard approach based on the total VZERO amplitude and the ZDC versus ZEM anti-correlation. The details of Table 1 are explained in the following paragraphs.

A related source of systematic error which affects 'satellite' vertices and hence only the FMD and VZERO analyses is the uncertainty of the ZEM scaling factors. This was evaluated by varying the ZEM scaling factors between the values obtained via a linear fit to the ZDC versus ZEM anti-correlation and the values which give the appropriate number of events in each centrality bin (i.e. the 0–5% bin should have the same number of events as the 5–10% bin and half the number of events of the 10–20% and 20–30% bins) and studying the effect on the final values. The influence of the particle composition, the particle spectra and the relative fraction of weak decays of Λ and K^0_s are studied by modifying these quantities within the Monte Carlo simulation in order to match the measured particle spectra and yields [21,22]. The uncertainty due to the description of the material budget in the region concerned by the analysis was estimated by varying the contribution of secondary particles from interactions in the detector material by 10%.

For the FMD, two detector-specific contributions to the systematic error are considered. First, the noise cut and clustering threshold, determining which strips have no or partial signals from particles, are varied by ±10%. This was found from simulations to be the range in which the probability to identify two particles as one and a single particle as multiple particles is minimal. The effect of these variations on the final result is a component of the systematic error. Secondly, an alternative method is used to determine the FMD multiplicity. The method using Poisson statistics is compared to a method using the distributions of deposited energy in the FMD. The difference between the results obtained by the two methods (2%) is an additional component of the systematic error.

The systematic error in the VZERO measurement stems mainly from the uncertainty of the SPD results used to calibrate the VZERO response. The systematic error related to the SPD analysis is described in detail in [16] and is the basis of the uncertainty on the VZERO calibration. A further contribution to the systematic error is assessed by taking into account the variation between the results from various VZERO rings at different 'satellite' vertices that cover the same or close pseudorapidity ranges.

5. Results

Figs. 2 and 3 show the resultant charged-particle pseudorapidity density from each of the three detectors individually and combined, respectively. The combined distribution is computed as the average value of $dN_{ch}/d\eta$ between the various detectors weighted by the systematic errors that are not common to the detectors (the statistical errors are negligible in comparison to the systematic errors). The error obtained from this weighting is then summed in quadrature with the common systematic errors. Finally, the distribution is symmetrized around $\eta = 0$ in the range of $|\eta| < 5$ by computing the average of $dN_{ch}/d\eta$ at positive and negative η values weighted by their systematic errors. This positive–negative asymmetry varies between 1% and 8%. The resultant distribution is in agreement with those measured by ATLAS [10] and CMS [9]. The lines on Fig. 3 represent fits to the following function:

$$A_1 e^{-\frac{\eta^2}{\sigma_1^2}} - A_2 e^{-\frac{\eta^2}{\sigma_2^2}},$$

that is the difference of two Gaussians centered at $\eta = 0$ and having amplitudes A_1, A_2 and widths σ_1, σ_2. For the 0–5% bin, $A_1 = 2102 \pm 105$, $A_2 = 485 \pm 99$, $\sigma_1 = 3.7 \pm 0.1$, and $\sigma_2 = 1.2 \pm 0.2$. The values of A_1/A_2, σ_1, and σ_2 are the same for each measured centrality bin within errors. This function describes the data well within the measured region and gives the best fit among multiple functions used to extrapolate the distribution to $\pm y_{beam}$ ($y_{beam} = 7.99$ at $\sqrt{s_{NN}} = 2.76$ TeV) in order to obtain the total charged-particle yield. The results of the extrapolation are summarized in Table 2 and Fig. 4. The extrapolation is performed using four different fit functions: the Gaussian function mentioned earlier, a trapezoidal function from [6], a function composed of a hyperbolic cosine and exponential also from [6], as well as a Bjorken inspired function composed of a central plateau with Gaussian tails. The central value of the extrapolation is derived from the trapezoidal function as little yield is expected beyond y_{beam}. The quoted errors include the variation of the fit parameters due to the

Table 2
The number of participants $\langle N_{part} \rangle$ estimated from the Glauber model [18] and the total charged-particle yield in the measured region ($-5.0 < \eta < 5.5$) and extrapolated to $\pm y_{beam}$ for different centrality fractions.

Centrality [%]	$\langle N_{part} \rangle$	$N_{ch,-5.0<\eta<5.5}$	$N_{ch,\|\eta\|\leqslant y_{beam}}$
0–5	382.8 ± 3.1	14 963 ± 666	17 165 ± 772
5–10	329.7 ± 4.6	12 272 ± 561	14 099 ± 655
10–20	260.5 ± 4.4	9205 ± 457	10 581 ± 535
20–30	186.4 ± 3.9	6324 ± 330	7278 ± 387

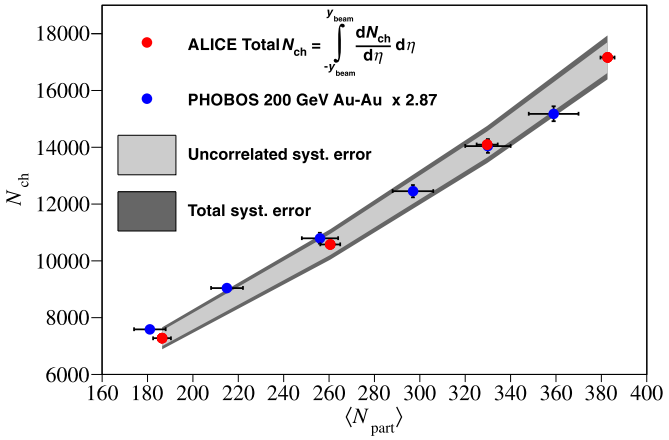

Fig. 4. Extrapolation to the total number of produced charged particles as a function of the number of participating nucleons. The light-gray band represents the uncorrelated errors from the extrapolation fit while the dark-gray band shows the increase to the total systematic errors which includes the common error coming from the uncertainty in the centrality estimation. The lower energy data from PHOBOS [6] was scaled by the average number of charged particles per participant with $\langle N_{part} \rangle > 180$ found in the ALICE measurements divided by the same quantity found in the PHOBOS measurements.

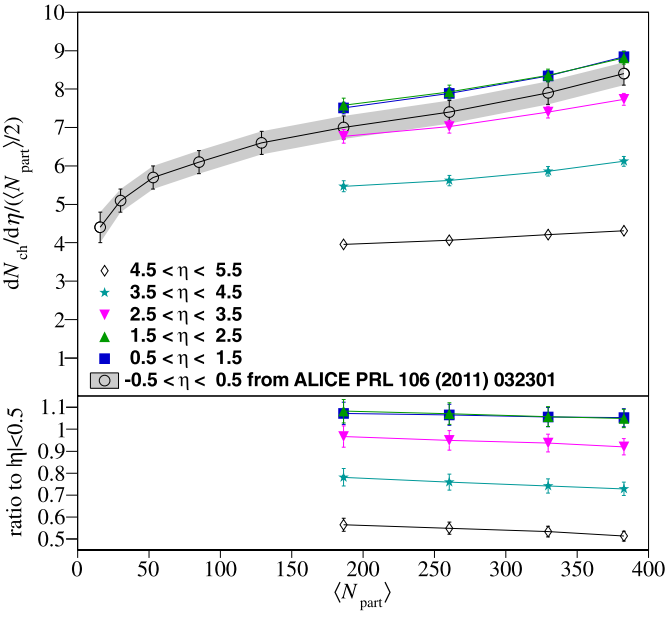

Fig. 5. $dN_{ch}/d\eta/(\langle N_{part} \rangle/2)$ as a function of $\langle N_{part} \rangle$ for different η ranges. The lower panel shows the ratio of each distribution to the published distribution from data with $|\eta| < 0.5$.

measurement uncertainties as well as the deviations between the four fit functions in the region beyond the pseudorapidity range covered by the experimental data. The total number of produced charged particles as a function of the number of participating nucleons shows a similar behavior as at lower energies when scaled to have the same average number of charged particles per participant (see Fig. 4).

In Fig. 5 we present the charged-particle pseudorapidity density per participating nucleon pair, $\langle N_{part} \rangle/2$, as a function of $\langle N_{part} \rangle$ for different pseudorapidity ranges. The lower panel of Fig. 5 shows no strong evolution in the shape of the pseudorapidity density distribution as a function of event centrality for the 30% most central events.

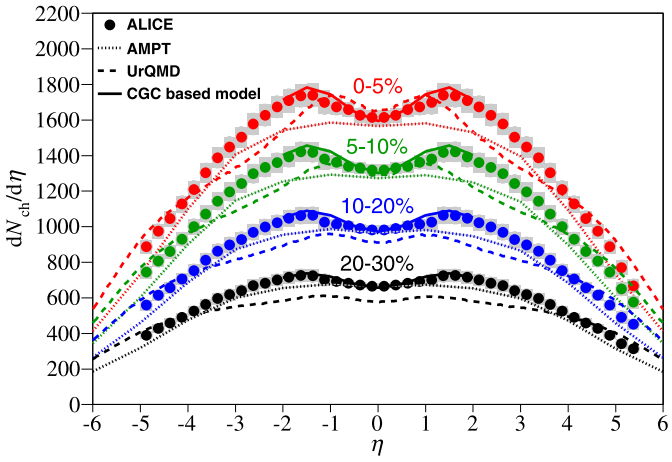

Fig. 6. $dN_{ch}/d\eta$ per centrality class compared to model predictions [23–27].

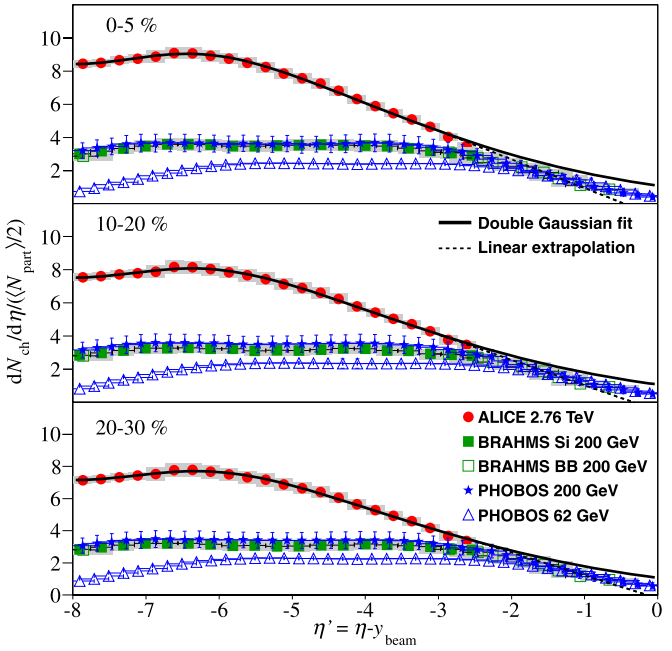

Fig. 7. The charged-particle pseudorapidity density distribution per participating nucleon pair for three centrality bins shown in the rest frame of one of the projectiles by using the variable $\eta' = \eta - y_{beam}$ ($y_{beam} = 7.99$). The ALICE results are extrapolated to further values of η' by fitting to the difference of two Gaussian functions (described earlier) and fitting a straight line to the last few points on the curve. These results are compared to lower energy data [6,12].

We have compared our measurement to three theoretical models which predict the pseudorapidity density – a Color Glass Condensate (CGC) based model [23,24], the UrQMD model [25], and the AMPT model [26] as tuned in [27]. As seen in Fig. 6, in its limited pseudorapidity range ($|\eta| < 2$) the CGC based model has a similar shape to the measured result. The UrQMD model gives a reasonable description of the region $|\eta| > 4$ and the shape at mid-rapidity, but is unable to describe the overall level of the pseudorapidity density as well as most of the shape. The AMPT model does reproduce the level at mid-rapidity as it was tuned for, but fails to reproduce the overall shape.

It is well established that up to RHIC energies the particle production in the fragmentation region is invariant with the beam energy [28]. This phenomenon is usually referred to as longitudinal scaling and is observed by plotting the particle yields with respect

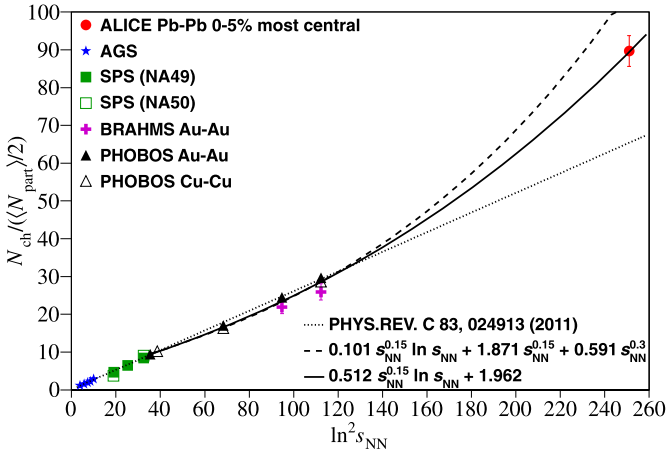

Fig. 8. Total $N_{\rm ch}$ per participant pair versus $\ln^2 s_{\rm NN}$. Also shown (dotted line) is the fit to the AGS [30,31], SPS [32,33], and RHIC [6,11,12] data from [6] using the trapezoidal approximation for $\mathrm{d}N_{\rm ch}/\mathrm{d}\eta$ and assuming that the mid-rapidity $\mathrm{d}N_{\rm ch}/\mathrm{d}\eta$ scales as $\ln s_{\rm NN}$. The dashed line is a fit to the RHIC and ALICE data derived using the trapezoidal approximation, but assuming the mid-rapidity $\mathrm{d}N_{\rm ch}/\mathrm{d}\eta$ scales as $s_{\rm NN}^{0.15}$ as in [8]. The full drawn line is a fit to the RHIC and ALICE data derived assuming that $\mathrm{d}N_{\rm ch}/\mathrm{d}\eta$ is dominated by a flat mid-rapidity region with a width that grows as $\ln s_{\rm NN}$.

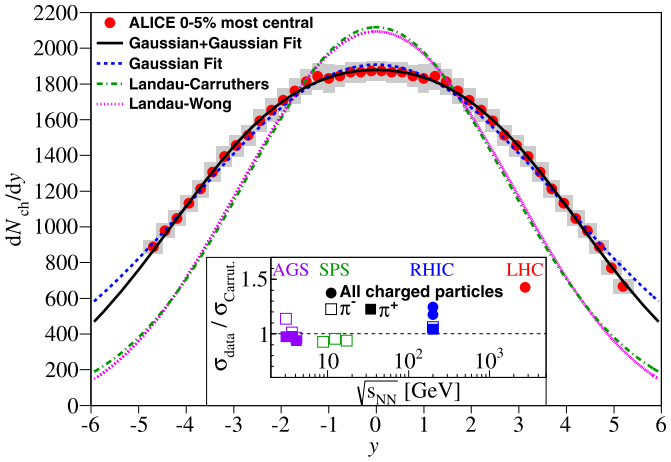

Fig. 9. $\mathrm{d}N_{\rm ch}/\mathrm{d}y$ distribution for the 5% most central Pb–Pb collisions. A Gaussian distribution has been fit to the data ($\sigma = 3.86$). A Landau–Carruthers Gaussian [35] and a Landau–Wong function [36] are also shown. The full drawn line shows a fit to the sum of two Gaussian distributions of equal widths with the means at $\eta = \pm 2.17$ and $\sigma = 2.6$ as its area reproduces the estimated total number of charged particles. The inset shows the energy dependence of the ratio of σ from a Gaussian fit to the expected Landau–Carruthers σ taken from [34] extended to $\sqrt{s_{\rm NN}} = 2.76$ TeV along with including RHIC points derived from the $\mathrm{d}N_{\rm ch}/\mathrm{d}\eta$ distributions measured by BRAHMS [12] and PHOBOS [29] converted to $\mathrm{d}N_{\rm ch}/\mathrm{d}y$ (the higher point and the lower point, respectively) using the same method employed at $\sqrt{s_{\rm NN}} = 2.76$ TeV.

to the variable $\eta - y_{\rm beam}$ [29]. As it can be seen from Fig. 7, our measurement is consistent with the validity of longitudinal scaling within the errors arising mainly from the extrapolation of the charged-particle pseudorapidity density from the measured region to the rapidity region of the projectile.

The number of produced charged particles per participant pair was observed to have a linear dependence on $\ln^2 s_{\rm NN}$ from AGS to RHIC energies based on a trapezoidal approximation for the $\mathrm{d}N_{\rm ch}/\mathrm{d}\eta$ distribution with $\mathrm{d}N_{\rm ch}/\mathrm{d}\eta$ at mid-rapidity increasing proportional to $\ln s_{\rm NN}$ [6]. Fig. 8 shows this trend together with the present ALICE measurement. The trend does not persist to LHC energies and underpredicts the total number of produced charged particles at $\sqrt{s_{\rm NN}} = 2.76$ TeV. To test if the trapezoidal approximation for the $\mathrm{d}N_{\rm ch}/\mathrm{d}\eta$ distribution is still valid using a power law scaling of the mid-rapidity $\mathrm{d}N_{\rm ch}/\mathrm{d}\eta$ [8], a new fit was performed to the RHIC and ALICE data, but was found to overpredict the total number of produced charged particles at $\sqrt{s_{\rm NN}} = 2.76$ TeV. Therefore, the trapezoidal approximation does not hold to LHC energies. Instead, a fit with a mid-rapidity $\mathrm{d}N_{\rm ch}/\mathrm{d}\eta$ value that scales as a power law as in [8] and extends over an η range scaling with $\ln s_{\rm NN}$ gives a better general description.

Fig. 9 shows the $\mathrm{d}N_{\rm ch}/\mathrm{d}y$ distribution versus y estimated by performing a Jacobian transformation from η to y utilizing the measured particle ratios and $p_{\rm T}$ distributions in ALICE for $\pi^{\pm}$, $K^{\pm}$, p, and $\bar{p}$ at mid-rapidity [21]. The systematic error on the estimate includes a linear softening of the $p_{\rm T}$ spectra with $|\eta|$ where the $\langle p_{\rm T}\rangle$ at $\eta = 3$ is 0.8 of the $\langle p_{\rm T}\rangle$ at $\eta = 0$ corresponding to approximately twice that seen for pions at RHIC [34]. The systematic error also includes variations in the particle ratios of $\pm 50\%$ beyond $\eta = 2.5$ and a linear reduction in these variations to 0 as $\eta \to 0$. The contribution from net-protons was neglected as they contribute predominately near beam rapidity and was, therefore, considered small relative to the variations in the other parameters. While the data, within systematic errors, are consistent with a flat rapidity plateau of about ± 1.5 units around $y = 0$, they are also well described over the full acceptance by a wide Gaussian distribution with $\sigma = 3.86$. This width, however, is larger than expected from Landau hydrodynamics [35,36]. Lower-energy distributions derived from identified pions have a width much closer to that expected from Landau hydrodynamics (see inset in Fig. 9). Two measurements derived from charged particles were computed using the $p_{\rm T}$ spectra and particle ratios measured by STAR [37] to convert the $\mathrm{d}N_{\rm ch}/\mathrm{d}\eta$ distributions measured by BRAHMS [12] and PHOBOS [29] to $\mathrm{d}N_{\rm ch}/\mathrm{d}y$ distributions in the same way as previously applied to the ALICE measurement. While the widths are larger than those derived from identified pions at $\sqrt{s_{\rm NN}} = 200$ GeV, there remains a significant increase from RHIC to LHC energies. Similar observations of deviations from Landau hydrodynamics have been seen in other Pb–Pb measurements at $\sqrt{s_{\rm NN}} = 2.76$ TeV [38].

6. Conclusions

The charged-particle pseudorapidity density distribution has been measured in Pb–Pb collisions at $\sqrt{s_{\rm NN}} = 2.76$ TeV. Results were obtained using a special sample of triggered 'satellite' collisions which allowed for reliable multiplicity measurements in the 0–30% centrality range. The measurement was performed in a wide pseudorapidity interval of $-5.0 < \eta < 5.5$ allowing for the first estimate of the total number of charged particles produced at the LHC. The available theoretical predictions do not describe the data satisfactorily although the CGC based model does well within its limited pseudorapidity range. We do not observe a significant change in the shape of the distributions as a function of the event centrality. Our results are compatible with the preservation of longitudinal scaling up to $\sqrt{s_{\rm NN}} = 2.76$ TeV. The scaling of total number of charged particles per participant pair with $\ln^2 s_{\rm NN}$ does not persist to LHC energies. The $\mathrm{d}N_{\rm ch}/\mathrm{d}y$ distribution of particles has a much larger width than that expected from Landau hydrodynamics, showing an increasing deviation at higher energies.

Acknowledgements

The ALICE collaboration would like to thank all its engineers and technicians for their invaluable contributions to the construction of the experiment and the CERN accelerator teams for the outstanding performance of the LHC complex.

The ALICE collaboration acknowledges the following funding agencies for their support in building and running the ALICE detector:

State Committee of Science, World Federation of Scientists (WFS) and Swiss Fonds Kidagan, Armenia;
Conselho Nacional de Desenvolvimento Científico e Tecnológico (CNPq), Financiadora de Estudos e Projetos (FINEP), Fundação de Amparo à Pesquisa do Estado de São Paulo (FAPESP);
National Natural Science Foundation of China (NSFC), the Chinese Ministry of Education (CMOE) and the Ministry of Science and Technology of China (MSTC);
Ministry of Education and Youth of the Czech Republic;
Danish Natural Science Research Council, the Carlsberg Foundation and the Danish National Research Foundation;
The European Research Council under the European Community's Seventh Framework Programme;
Helsinki Institute of Physics and the Academy of Finland;
French CNRS-IN2P3, the 'Region Pays de Loire', 'Region Alsace', 'Region Auvergne' and CEA, France;
German BMBF and the Helmholtz Association;
General Secretariat for Research and Technology, Ministry of Development, Greece;
Hungarian OTKA and National Office for Research and Technology (NKTH);
Department of Atomic Energy and Department of Science and Technology of the Government of India;
Istituto Nazionale di Fisica Nucleare (INFN) and Centro Fermi – Museo Storico della Fisica e Centro Studi e Ricerche "Enrico Fermi", Italy;
MEXT Grant-in-Aid for Specially Promoted Research, Japan;
Joint Institute for Nuclear Research, Dubna;
National Research Foundation of Korea (NRF);
CONACYT, DGAPA, México, ALFA-EC and the EPLANET Program (European Particle Physics Latin American Network);
Stichting voor Fundamenteel Onderzoek der Materie (FOM) and the Nederlandse Organisatie voor Wetenschappelijk Onderzoek (NWO), Netherlands;
Research Council of Norway (NFR);
Polish Ministry of Science and Higher Education;
National Authority for Scientific Research – NASR (Autoritatea Naţională pentru Cercetare Ştiinţifică – ANCS);
Ministry of Education and Science of Russian Federation, Russian Academy of Sciences, Russian Federal Agency of Atomic Energy, Russian Federal Agency for Science and Innovations and the Russian Foundation for Basic Research;
Ministry of Education of Slovakia;
Department of Science and Technology, South Africa;
CIEMAT, EELA, Ministerio de Economía y Competitividad (MINECO) of Spain, Xunta de Galicia (Consellería de Educación), CEADEN, Cubaenergía, Cuba, and IAEA (International Atomic Energy Agency);
Swedish Research Council (VR) and Knut & Alice Wallenberg Foundation (KAW);
Ukraine Ministry of Education and Science;
United Kingdom Science and Technology Facilities Council (STFC);
The United States Department of Energy, the United States National Science Foundation, the State of Texas, and the State of Ohio.

Open access

References

[1] I. Arsene, et al., Quark–gluon plasma and color glass condensate at RHIC? The perspective from the BRAHMS experiment, Nucl. Phys. A 757 (2005) 1–27, http://dx.doi.org/10.1016/j.nuclphysa.2005.02.130, arXiv:nucl-ex/0410020.
[2] B.B. Back, et al., The PHOBOS perspective on discoveries at RHIC, Nucl. Phys. A 757 (2005) 28–101, http://dx.doi.org/10.1016/j.nuclphysa.2005.03.084, arXiv:nucl-ex/0410022.
[3] J. Adams, et al., Experimental and theoretical challenges in the search for the quark gluon plasma: The STAR Collaboration's critical assessment of the evidence from RHIC collisions, Nucl. Phys. A 757 (2005) 102–183, http://dx.doi.org/10.1016/j.nuclphysa.2005.03.085, arXiv:nucl-ex/0501009.
[4] K. Adcox, et al., Formation of dense partonic matter in relativistic nucleus–nucleus collisions at RHIC: Experimental evaluation by the PHENIX Collaboration, Nucl. Phys. A 757 (2005) 184–283, http://dx.doi.org/10.1016/j.nuclphysa.2005.03.086, arXiv:nucl-ex/0410003.
[5] L.V. Gribov, E.M. Levin, M.G. Ryskin, Semihard processes in QCD, Phys. Rep. 100 (1983) 1–150, http://dx.doi.org/10.1016/0370-1573(83)90022-4.
[6] B. Alver, et al., Charged-particle multiplicity and pseudorapidity distributions measured with the PHOBOS detector in Au + Au, Cu + Cu, **d** + Au, and **p** + **p** collisions at ultrarelativistic energies, Phys. Rev. C 83 (2011) 024913, http://dx.doi.org/10.1103/PhysRevC.83.024913, arXiv:1011.1940.
[7] B.B. Back, et al., Charged-particle pseudorapidity distributions in Au + Au collisions at $\sqrt{s_{NN}} = 62.4$ GeV, Phys. Rev. C 74 (2006) 021901, http://dx.doi.org/10.1103/PhysRevC.74.021901, arXiv:nucl-ex/0509034.
[8] K. Aamodt, et al., Charged-particle multiplicity density at midrapidity in central Pb–Pb collisions at $\sqrt{s_{NN}} = 2.76$ TeV, Phys. Rev. Lett. 105 (2010) 252301, http://dx.doi.org/10.1103/PhysRevLett.105.252301, arXiv:1011.3916.
[9] S. Chatrchyan, et al., Dependence on pseudorapidity and on centrality of charged hadron production in PbPb collisions at $\sqrt{s_{NN}} = 2.76$ TeV, J. High Energy Phys. 1108 (2011) 141, http://dx.doi.org/10.1007/JHEP08(2011)141, arXiv:1107.4800.
[10] G. Aad, et al., Measurement of the centrality dependence of the charged particle pseudorapidity distribution in lead-lead collisions at $\sqrt{s_{NN}} = 2.76$ TeV with the ATLAS detector, Phys. Lett. B 710 (2012) 363–382, http://dx.doi.org/10.1016/j.physletb.2012.02.045, arXiv:1108.6027.
[11] I.G. Bearden, et al., Charged particle densities from Au + Au collisions at $\sqrt{s_{NN}} = 130$ GeV, Phys. Lett. B 523 (2001) 227–233, http://dx.doi.org/10.1016/S0370-2693(01)01333-8, arXiv:nucl-ex/0108016.
[12] I.G. Bearden, et al., Pseudorapidity distributions of charged particles from Au + Au collisions at the maximum RHIC energy, $\sqrt{s_{NN}} = 200$ GeV, Phys. Rev. Lett. 88 (2002) 202301, http://dx.doi.org/10.1103/PhysRevLett.88.202301, arXiv:nucl-ex/0112001.
[13] K. Aamodt, et al., The ALICE experiment at the CERN LHC, J. Instrum. 3 (2008) S08002, http://dx.doi.org/10.1088/1748-0221/3/08/S08002.
[14] E. Abbas, et al., Performance of the ALICE VZERO system, arXiv:1306.3130.
[15] C.H. Christensen, et al., The ALICE forward multiplicity detector, Int. J. Mod. Phys. E 16 (2007) 2432–2437, http://dx.doi.org/10.1142/S0218301307008057, arXiv:0712.1117.
[16] K. Aamodt, et al., Centrality dependence of the charged-particle multiplicity density at midrapidity in Pb–Pb collisions at $\sqrt{s_{NN}} = 2.76$ TeV, Phys. Rev. Lett. 106 (2011) 032301, http://dx.doi.org/10.1103/PhysRevLett.106.032301, arXiv:1012.1657.
[17] A. Jeff, et al., Measurement of satellite bunches at the LHC, Conf. Proc. C 1205201 (2012) 97–99.
[18] B. Abelev, et al., Centrality determination of Pb–Pb collisions at $\sqrt{s_{NN}} = 2.76$ TeV with ALICE, arXiv:1301.4361.
[19] R. Brun, F. Carminati, S. Giani, GEANT detector description and simulation tool, CERN-W5013.
[20] X.-N. Wang, M. Gyulassy, HIJING: A Monte Carlo model for multiple jet production in pp, pA, and AA collisions, Phys. Rev. D 44 (1991) 3501–3516, http://dx.doi.org/10.1103/PhysRevD.44.3501.
[21] B. Abelev, et al., Pion, kaon, and proton production in central Pb–Pb collisions at $\sqrt{s_{NN}} = 2.76$ TeV, Phys. Rev. Lett. 109 (2012) 252301, http://dx.doi.org/10.1103/PhysRevLett.109.252301, arXiv:1208.1974.
[22] B. Abelev, et al., K^0_S and Λ production in Pb–Pb collisions at $\sqrt{s_{NN}} = 2.76$ TeV, arXiv:1307.5530.
[23] J.L. Albacete, A. Dumitru, A model for gluon production in heavy-ion collisions at the LHC with rcBK unintegrated gluon densities, arXiv:1011.5161.
[24] J.L. Albacete, A. Dumitru, Y. Nara, CGC initial conditions at RHIC and LHC, J. Phys. Conf. Ser. 316 (2011) 012011, http://dx.doi.org/10.1088/1742-6596/316/1/012011, arXiv:1106.0978.
[25] M. Mitrovski, T. Schuster, G. Graf, H. Petersen, M. Bleicher, Charged-particle (pseudo-)rapidity distributions in $p + \bar{p}/p + p$ and Pb + Pb/Au + Au colli-

sions from UrQMD calculations at energies available at the CERN super proton synchrotron to the large hadron collider, Phys. Rev. C 79 (2009) 044901, http://dx.doi.org/10.1103/PhysRevC.79.044901, arXiv:0812.2041.
[26] Z.-W. Lin, C.M. Ko, B.-A. Li, B. Zhang, S. Pal, A multi-phase transport model for relativistic heavy ion collisions, Phys. Rev. C 72 (2005) 064901, http://dx.doi.org/10.1103/PhysRevC.72.064901, arXiv:nucl-th/0411110.
[27] J. Xu, C.M. Ko, Pb–Pb collisions at $\sqrt{s_{NN}} = 2.76$ TeV in a multiphase transport model, Phys. Rev. C 83 (2011) 034904, http://dx.doi.org/10.1103/PhysRevC.83.034904, arXiv:1101.2231.
[28] J. Benecke, T.T. Chou, C.-N. Yang, E. Yen, Hypothesis of limiting fragmentation in high-energy collisions, Phys. Rev. 188 (1969) 2159–2169, http://dx.doi.org/10.1103/PhysRev.188.2159.
[29] B.B. Back, et al., The significance of the fragmentation region in ultrarelativistic heavy ion collisions, Phys. Rev. Lett. 91 (2003) 052303, http://dx.doi.org/10.1103/PhysRevLett.91.052303, arXiv:nucl-ex/0210015.
[30] J.L. Klay, et al., Charged pion production in 2*A* to 8*A* GeV central Au + Au collisions, Phys. Rev. C 68 (2003) 054905, http://dx.doi.org/10.1103/PhysRevC.68.054905, arXiv:nucl-ex/0306033.
[31] L. Ahle, et al., Particle production at high baryon density in central Au + Au reactions at 11.6*A* GeV/*c*, Phys. Rev. C 57 (1998) R466–R470, http://dx.doi.org/10.1103/PhysRevC.57.R466.
[32] S.V. Afanasiev, et al., Energy dependence of pion and kaon production in central Pb + Pb collisions, Phys. Rev. C 66 (2002) 054902, http://dx.doi.org/10.1103/PhysRevC.66.054902, arXiv:nucl-ex/0205002.
[33] M.C. Abreu, et al., Scaling of charged particle multiplicity in Pb–Pb collisions at SPS energies, Phys. Lett. B 530 (2002) 43–55, http://dx.doi.org/10.1016/S0370-2693(02)01353-9.
[34] I.G. Bearden, et al., Charged meson rapidity distributions in central Au + Au collisions at $\sqrt{s_{NN}} = 200$ GeV, Phys. Rev. Lett. 94 (2005) 162301, http://dx.doi.org/10.1103/PhysRevLett.94.162301, arXiv:nucl-ex/0403050.
[35] P. Carruthers, M. Duong-Van, New scaling law based on the hydrodynamical model of particle production, Phys. Lett. B 41 (1972) 597–601, http://dx.doi.org/10.1016/0370-2693(72)90643-0.
[36] C.-Y. Wong, Landau hydrodynamics reexamined, Phys. Rev. C 78 (2008) 054902, http://dx.doi.org/10.1103/PhysRevC.78.054902, arXiv:0808.1294.
[37] J. Adams, et al., Identified particle distributions in *pp* and Au + Au collisions at $\sqrt{s_{NN}} = 200$ GeV, Phys. Rev. Lett. 92 (2004) 112301, http://dx.doi.org/10.1103/PhysRevLett.92.112301, arXiv:nucl-ex/0310004.
[38] S. Chatrchyan, et al., Measurement of the pseudorapidity and centrality dependence of the transverse energy density in Pb–Pb collisions at $\sqrt{s_{NN}} = 2.76$ TeV, Phys. Rev. Lett. 109 (2012) 152303, http://dx.doi.org/10.1103/PhysRevLett.109.152303, arXiv:1205.2488.

ALICE Collaboration

E. Abbas [a], B. Abelev [bt], J. Adam [al], D. Adamová [ca], A.M. Adare [dz], M.M. Aggarwal [ce], G. Aglieri Rinella [ah], M. Agnello [cv,ck], A.G. Agocs [dy], A. Agostinelli [ab], Z. Ahammed [dt], A. Ahmad Masoodi [r], N. Ahmad [r], S.U. Ahn [bm], S.A. Ahn [bm], I. Aimo [y,cv,ck], M. Ajaz [p], A. Akindinov [ay], D. Aleksandrov [cq], B. Alessandro [cv], A. Alici [cx,m], A. Alkin [d], E. Almaráz Aviña [bi], J. Alme [aj], T. Alt [an], V. Altini [af], S. Altinpinar [s], I. Altsybeev [dv], C. Andrei [bw], A. Andronic [cn], V. Anguelov [cj], J. Anielski [bg], C. Anson [t], T. Antičić [co], F. Antinori [cw], P. Antonioli [cx], L. Aphecetche [dd], H. Appelshäuser [be], N. Arbor [bp], S. Arcelli [ab], A. Arend [be], N. Armesto [q], R. Arnaldi [cv], T. Aronsson [dz], I.C. Arsene [cn], M. Arslandok [be], A. Asryan [dv], A. Augustinus [ah], R. Averbeck [cn], T.C. Awes [cb], J. Äystö [aq], M.D. Azmi [r,cg], M. Bach [an], A. Badalà [cu], Y.W. Baek [bo,ao], R. Bailhache [be], R. Bala [ch,cv], A. Baldisseri [o], F. Baltasar Dos Santos Pedrosa [ah], J. Bán [az], R.C. Baral [ba], R. Barbera [aa], F. Barile [af], G.G. Barnaföldi [dy], L.S. Barnby [cs], V. Barret [bo], J. Bartke [dh], M. Basile [ab], N. Bastid [bo], S. Basu [dt], B. Bathen [bg], G. Batigne [dd], B. Batyunya [bk], P.C. Batzing [v], C. Baumann [be], I.G. Bearden [by], H. Beck [be], N.K. Behera [as], I. Belikov [bj], F. Bellini [ab], R. Bellwied [dn], E. Belmont-Moreno [bi], G. Bencedi [dy], S. Beole [y], I. Berceanu [bw], A. Bercuci [bw], Y. Berdnikov [cc], D. Berenyi [dy], A.A.E. Bergognon [dd], R.A. Bertens [ax], D. Berzano [y,cv], L. Betev [ah], A. Bhasin [ch], A.K. Bhati [ce], J. Bhom [dr], N. Bianchi [bq], L. Bianchi [y], C. Bianchin [ax], J. Bielčík [al], J. Bielčíková [ca], A. Bilandzic [by], S. Bjelogrlic [ax], F. Blanco [k], F. Blanco [dn], D. Blau [cq], C. Blume [be], M. Boccioli [ah], S. Böttger [bd], A. Bogdanov [bu], H. Bøggild [by], M. Bogolyubsky [av], L. Boldizsár [dy], M. Bombara [am], J. Book [be], H. Borel [o], A. Borissov [dx], F. Bossú [cg], M. Botje [bz], E. Botta [y], E. Braidot [bs], P. Braun-Munzinger [cn], M. Bregant [dd], T. Breitner [bd], T.A. Broker [be], T.A. Browning [cl], M. Broz [ak], R. Brun [ah], E. Bruna [y,cv], G.E. Bruno [af], D. Budnikov [cp], H. Buesching [be], S. Bufalino [y,cv], P. Buncic [ah], O. Busch [cj], Z. Buthelezi [cg], D. Caffarri [ac,cw], X. Cai [h], H. Caines [dz], E. Calvo Villar [ct], P. Camerini [w], V. Canoa Roman [l], G. Cara Romeo [cx], F. Carena [ah], W. Carena [ah], N. Carlin Filho [dk], F. Carminati [ah], A. Casanova Díaz [bq], J. Castillo Castellanos [o], J.F. Castillo Hernandez [cn], E.A.R. Casula [x], V. Catanescu [bw], C. Cavicchioli [ah], C. Ceballos Sanchez [j], J. Cepila [al], P. Cerello [cv], B. Chang [aq,eb], S. Chapeland [ah], J.L. Charvet [o], S. Chattopadhyay [dt], S. Chattopadhyay [cr], M. Cherney [cd], C. Cheshkov [ah,dm], B. Cheynis [dm], V. Chibante Barroso [ah], D.D. Chinellato [dn], P. Chochula [ah], M. Chojnacki [by], S. Choudhury [dt], P. Christakoglou [bz], C.H. Christensen [by], P. Christiansen [ag], T. Chujo [dr], S.U. Chung [cm], C. Cicalo [cy], L. Cifarelli [ab,m], F. Cindolo [cx], J. Cleymans [cg], F. Colamaria [af], D. Colella [af], A. Collu [x], G. Conesa Balbastre [bp], Z. Conesa del Valle [ah,au], M.E. Connors [dz], G. Contin [w], J.G. Contreras [l], T.M. Cormier [dx], Y. Corrales Morales [y], P. Cortese [ae], I. Cortés Maldonado [c], M.R. Cosentino [bs], F. Costa [ah], M.E. Cotallo [k], E. Crescio [l], P. Crochet [bo], E. Cruz Alaniz [bi],

R. Cruz Albino [l], E. Cuautle [bh], L. Cunqueiro [bq], A. Dainese [ac,cw], H.H. Dalsgaard [by], R. Dang [h], A. Danu [bc], K. Das [cr], I. Das [au], S. Das [e], D. Das [cr], A. Dash [dl], S. Dash [as], S. De [dt], G.O.V. de Barros [dk], A. De Caro [ad,m], G. de Cataldo [da], J. de Cuveland [an], A. De Falco [x], D. De Gruttola [ad,m], H. Delagrange [dd], A. Deloff [bv], N. De Marco [cv], E. Dénes [dy], S. De Pasquale [ad], A. Deppman [dk], G. D Erasmo [af], R. de Rooij [ax], M.A. Diaz Corchero [k], D. Di Bari [af], T. Dietel [bg], C. Di Giglio [af], S. Di Liberto [db], A. Di Mauro [ah], P. Di Nezza [bq], R. Divià [ah], Ø. Djuvsland [s], A. Dobrin [dx,ag,ax], T. Dobrowolski [bv], B. Dönigus [cn], O. Dordic [v], O. Driga [dd], A.K. Dubey [dt], A. Dubla [ax], L. Ducroux [dm], P. Dupieux [bo], A.K. Dutta Majumdar [cr], D. Elia [da], D. Emschermann [bg], H. Engel [bd], B. Erazmus [ah,dd], H.A. Erdal [aj], D. Eschweiler [an], B. Espagnon [au], M. Estienne [dd], S. Esumi [dr], D. Evans [cs], S. Evdokimov [av], G. Eyyubova [v], D. Fabris [ac,cw], J. Faivre [bp], D. Falchieri [ab], A. Fantoni [bq], M. Fasel [cj], D. Fehlker [s], L. Feldkamp [bg], D. Felea [bc], A. Feliciello [cv], B. Fenton-Olsen [bs], G. Feofilov [dv], A. Fernández Téllez [c], A. Ferretti [y], A. Festanti [ac], J. Figiel [dh], M.A.S. Figueredo [dk], S. Filchagin [cp], D. Finogeev [aw], F.M. Fionda [af], E.M. Fiore [af], E. Floratos [cf], M. Floris [ah], S. Foertsch [cg], P. Foka [cn], S. Fokin [cq], E. Fragiacomo [cz], A. Francescon [ah,ac], U. Frankenfeld [cn], U. Fuchs [ah], C. Furget [bp], M. Fusco Girard [ad], J.J. Gaardhøje [by], M. Gagliardi [y], A. Gago [ct], M. Gallio [y], D.R. Gangadharan [t], P. Ganoti [cb], C. Garabatos [cn], E. Garcia-Solis [n], C. Gargiulo [ah], I. Garishvili [bt], J. Gerhard [an], M. Germain [dd], C. Geuna [o], A. Gheata [ah], M. Gheata [bc,ah], B. Ghidini [af], P. Ghosh [dt], P. Gianotti [bq], M.R. Girard [dw], P. Giubellino [ah], E. Gladysz-Dziadus [dh], P. Glässel [cj], R. Gomez [dj,l], E.G. Ferreiro [q], L.H. González-Trueba [bi], P. González-Zamora [k], S. Gorbunov [an], A. Goswami [ci], S. Gotovac [df], L.K. Graczykowski [dw], R. Grajcarek [cj], A. Grelli [ax], A. Grigoras [ah], C. Grigoras [ah], V. Grigoriev [bu], A. Grigoryan [b], S. Grigoryan [bk], B. Grinyov [d], N. Grion [cz], P. Gros [ag], J.F. Grosse-Oetringhaus [ah], J.-Y. Grossiord [dm], R. Grosso [ah], F. Guber [aw], R. Guernane [bp], B. Guerzoni [ab], M. Guilbaud [dm], K. Gulbrandsen [by], H. Gulkanyan [b], T. Gunji [dq], R. Gupta [ch], A. Gupta [ch], R. Haake [bg], Ø. Haaland [s], C. Hadjidakis [au], M. Haiduc [bc], H. Hamagaki [dq], G. Hamar [dy], B.H. Han [u], L.D. Hanratty [cs], A. Hansen [by], Z. Harmanová-Tóthová [am], J.W. Harris [dz], M. Hartig [be], A. Harton [n], D. Hatzifotiadou [cx], S. Hayashi [dq], A. Hayrapetyan [ah,b], S.T. Heckel [be], M. Heide [bg], H. Helstrup [aj], A. Herghelegiu [bw], G. Herrera Corral [l], N. Herrmann [cj], B.A. Hess [ds], K.F. Hetland [aj], B. Hicks [dz], B. Hippolyte [bj], Y. Hori [dq], P. Hristov [ah], I. Hřivnáčová [au], M. Huang [s], T.J. Humanic [t], D.S. Hwang [u], R. Ichou [bo], R. Ilkaev [cp], I. Ilkiv [bv], M. Inaba [dr], E. Incani [x], P.G. Innocenti [ah], G.M. Innocenti [y], M. Ippolitov [cq], M. Irfan [r], C. Ivan [cn], V. Ivanov [cc], A. Ivanov [dv], M. Ivanov [cn], O. Ivanytskyi [d], A. Jachołkowski [aa], P.M. Jacobs [bs], C. Jahnke [dk], H.J. Jang [bm], M.A. Janik [dw], P.H.S.Y. Jayarathna [dn], S. Jena [as], D.M. Jha [dx], R.T. Jimenez Bustamante [bh], P.G. Jones [cs], H. Jung [ao], A. Jusko [cs], A.B. Kaidalov [ay], S. Kalcher [an], P. Kaliňák [az], T. Kalliokoski [aq], A. Kalweit [ah], J.H. Kang [eb], V. Kaplin [bu], S. Kar [dt], A. Karasu Uysal [ah,ea,bn], O. Karavichev [aw], T. Karavicheva [aw], E. Karpechev [aw], A. Kazantsev [cq], U. Kebschull [bd], R. Keidel [ec], B. Ketzer [be,dg], K.H. Khan [p], M.M. Khan [r], P. Khan [cr], S.A. Khan [dt], A. Khanzadeev [cc], Y. Kharlov [av], B. Kileng [aj], M. Kim [eb], S. Kim [u], B. Kim [eb], T. Kim [eb], D.J. Kim [aq], D.W. Kim [ao,bm], J.H. Kim [u], J.S. Kim [ao], M. Kim [ao], S. Kirsch [an], I. Kisel [an], S. Kiselev [ay], A. Kisiel [dw], J.L. Klay [g], J. Klein [cj], C. Klein-Bösing [bg], M. Kliemant [be], A. Kluge [ah], M.L. Knichel [cn], A.G. Knospe [di], M.K. Köhler [cn], T. Kollegger [an], A. Kolojvari [dv], M. Kompaniets [dv], V. Kondratiev [dv], N. Kondratyeva [bu], A. Konevskikh [aw], V. Kovalenko [dv], M. Kowalski [dh], S. Kox [bp], G. Koyithatta Meethaleveedu [as], J. Kral [aq], I. Králik [az], F. Kramer [be], A. Kravčáková [am], M. Krelina [al], M. Kretz [an], M. Krivda [cs,az], F. Krizek [aq], M. Krus [al], E. Kryshen [cc], M. Krzewicki [cn], V. Kucera [ca], Y. Kucheriaev [cq], T. Kugathasan [ah], C. Kuhn [bj], P.G. Kuijer [bz], I. Kulakov [be], J. Kumar [as], P. Kurashvili [bv], A. Kurepin [aw], A.B. Kurepin [aw], A. Kuryakin [cp], S. Kushpil [ca], V. Kushpil [ca], H. Kvaerno [v], M.J. Kweon [cj], Y. Kwon [eb], P. Ladrón de Guevara [bh], I. Lakomov [au], R. Langoy [s,du], S.L. La Pointe [ax], C. Lara [bd], A. Lardeux [dd], P. La Rocca [aa], R. Lea [w], M. Lechman [ah], S.C. Lee [ao], G.R. Lee [cs], I. Legrand [ah], J. Lehnert [be], R.C. Lemmon [dc], M. Lenhardt [cn], V. Lenti [da], H. León [bi], M. Leoncino [y], I. León Monzón [dj], P. Lévai [dy], S. Li [bo,h], J. Lien [s,du], R. Lietava [cs],

S. Lindal [v], V. Lindenstruth [an], C. Lippmann [cn,ah], M.A. Lisa [t], H.M. Ljunggren [ag], D.F. Lodato [ax], P.I. Loenne [s], V.R. Loggins [dx], V. Loginov [bu], D. Lohner [cj], C. Loizides [bs], K.K. Loo [aq], X. Lopez [bo], E. López Torres [j], G. Løvhøiden [v], X.-G. Lu [cj], P. Luettig [be], M. Lunardon [ac], J. Luo [h], G. Luparello [ax], C. Luzzi [ah], K. Ma [h], R. Ma [dz], D.M. Madagodahettige-Don [dn], A. Maevskaya [aw], M. Mager [bf,ah], D.P. Mahapatra [ba], A. Maire [cj], M. Malaev [cc], I. Maldonado Cervantes [bh], Ludmila Malinina [bk,1], D. Mal'Kevich [ay], P. Malzacher [cn], A. Mamonov [cp], L. Manceau [cv], L. Mangotra [ch], V. Manko [cq], F. Manso [bo], V. Manzari [da], Y. Mao [h], M. Marchisone [bo,y], J. Mareš [bb], G.V. Margagliotti [w,cz], A. Margotti [cx], A. Marín [cn], C. Markert [di], M. Marquard [be], I. Martashvili [dp], N.A. Martin [cn], P. Martinengo [ah], M.I. Martínez [c], G. Martínez García [dd], Y. Martynov [d], A. Mas [dd], S. Masciocchi [cn], M. Masera [y], A. Masoni [cy], L. Massacrier [dd], A. Mastroserio [af], A. Matyja [dh], C. Mayer [dh], J. Mazer [dp], M.A. Mazzoni [db], F. Meddi [z], A. Menchaca-Rocha [bi], J. Mercado Pérez [cj], M. Meres [ak], Y. Miake [dr], K. Mikhaylov [bk,ay], L. Milano [ah,y], Jovan Milosevic [v,2], A. Mischke [ax], A.N. Mishra [ci,at], D. Miśkowiec [cn], C. Mitu [bc], S. Mizuno [dr], J. Mlynarz [dx], B. Mohanty [dt,bx], L. Molnar [dy,bj], L. Montaño Zetina [l], M. Monteno [cv], E. Montes [k], T. Moon [eb], M. Morando [ac], D.A. Moreira De Godoy [dk], S. Moretto [ac], A. Morreale [aq], A. Morsch [ah], V. Muccifora [bq], E. Mudnic [df], S. Muhuri [dt], M. Mukherjee [dt], H. Müller [ah], M.G. Munhoz [dk], S. Murray [cg], L. Musa [ah], J. Musinsky [az], B.K. Nandi [as], R. Nania [cx], E. Nappi [da], C. Nattrass [dp], T.K. Nayak [dt], S. Nazarenko [cp], A. Nedosekin [ay], M. Nicassio [af,cn], M. Niculescu [bc,ah], B.S. Nielsen [by], T. Niida [dr], S. Nikolaev [cq], V. Nikolic [co], S. Nikulin [cq], V. Nikulin [cc], B.S. Nilsen [cd], M.S. Nilsson [v], F. Noferini [cx,m], P. Nomokonov [bk], G. Nooren [ax], A. Nyanin [cq], A. Nyatha [as], C. Nygaard [by], J. Nystrand [s], A. Ochirov [dv], H. Oeschler [bf,ah,cj], S. Oh [dz], S.K. Oh [ao], J. Oleniacz [dw], A.C. Oliveira Da Silva [dk], C. Oppedisano [cv], A. Ortiz Velasquez [ag,bh], A. Oskarsson [ag], P. Ostrowski [dw], J. Otwinowski [cn], K. Oyama [cj], K. Ozawa [dq], Y. Pachmayer [cj], M. Pachr [al], F. Padilla [y], P. Pagano [ad], G. Paić [bh], F. Painke [an], C. Pajares [q], S.K. Pal [dt], A. Palaha [cs], A. Palmeri [cu], V. Papikyan [b], G.S. Pappalardo [cu], W.J. Park [cn], A. Passfeld [bg], D.I. Patalakha [av], V. Paticchio [da], B. Paul [cr], A. Pavlinov [dx], T. Pawlak [dw], T. Peitzmann [ax], H. Pereira Da Costa [o], E. Pereira De Oliveira Filho [dk], D. Peresunko [cq], C.E. Pérez Lara [bz], D. Perrino [af], W. Peryt [dw], A. Pesci [cx], Y. Pestov [f], V. Petráček [al], M. Petran [al], M. Petris [bw], P. Petrov [cs], M. Petrovici [bw], C. Petta [aa], S. Piano [cz], M. Pikna [ak], P. Pillot [dd], O. Pinazza [ah], L. Pinsky [dn], N. Pitz [be], D.B. Piyarathna [dn], M. Planinic [co], M. Płoskoń [bs], J. Pluta [dw], T. Pocheptsov [bk], S. Pochybova [dy], P.L.M. Podesta-Lerma [dj], M.G. Poghosyan [ah], K. Polák [bb], B. Polichtchouk [av], N. Poljak [ax,co], A. Pop [bw], S. Porteboeuf-Houssais [bo], V. Pospíšil [al], B. Potukuchi [ch], S.K. Prasad [dx], R. Preghenella [cx,m], F. Prino [cv], C.A. Pruneau [dx], I. Pshenichnov [aw], G. Puddu [x], V. Punin [cp], M. Putiš [am], J. Putschke [dx], H. Qvigstad [v], A. Rachevski [cz], A. Rademakers [ah], T.S. Räihä [aq], J. Rak [aq], A. Rakotozafindrabe [o], L. Ramello [ae], S. Raniwala [ci], R. Raniwala [ci], S.S. Räsänen [aq], B.T. Rascanu [be], D. Rathee [ce], W. Rauch [ah], K.F. Read [dp], J.S. Real [bp], K. Redlich [bv,3], R.J. Reed [dz], A. Rehman [s], P. Reichelt [be], M. Reicher [ax], R. Renfordt [be], A.R. Reolon [bq], A. Reshetin [aw], F. Rettig [an], J.-P. Revol [ah], K. Reygers [cj], L. Riccati [cv], R.A. Ricci [br], T. Richert [ag], M. Richter [v], P. Riedler [ah], W. Riegler [ah], F. Riggi [aa,cu], M. Rodríguez Cahuantzi [c], A. Rodriguez Manso [bz], K. Røed [s,v], E. Rogochaya [bk], D. Rohr [an], D. Röhrich [s], R. Romita [cn,dc], F. Ronchetti [bq], P. Rosnet [bo], S. Rossegger [ah], A. Rossi [ah,ac], P. Roy [cr], C. Roy [bj], A.J. Rubio Montero [k], R. Rui [w], R. Russo [y], E. Ryabinkin [cq], A. Rybicki [dh], S. Sadovsky [av], K. Šafařík [ah], R. Sahoo [at], P.K. Sahu [ba], J. Saini [dt], H. Sakaguchi [ar], S. Sakai [bs], D. Sakata [dr], C.A. Salgado [q], J. Salzwedel [t], S. Sambyal [ch], V. Samsonov [cc], X. Sanchez Castro [bj], L. Šándor [az], A. Sandoval [bi], M. Sano [dr], G. Santagati [aa], R. Santoro [ah,m], J. Sarkamo [aq], D. Sarkar [dt], E. Scapparone [cx], F. Scarlassara [ac], R.P. Scharenberg [cl], C. Schiaua [bw], R. Schicker [cj], H.R. Schmidt [ds], C. Schmidt [cn], S. Schuchmann [be], J. Schukraft [ah], T. Schuster [dz], Y. Schutz [ah,dd], K. Schwarz [cn], K. Schweda [cn], G. Scioli [ab], E. Scomparin [cv], R. Scott [dp], P.A. Scott [cs], G. Segato [ac], I. Selyuzhenkov [cn], S. Senyukov [bj], J. Seo [cm], S. Serci [x], E. Serradilla [k,bi], A. Sevcenco [bc], A. Shabetai [dd], G. Shabratova [bk],

R. Shahoyan [ah], N. Sharma [dp], S. Sharma [ch], S. Rohni [ch], K. Shigaki [ar], K. Shtejer [j], Y. Sibiriak [cq], E. Sicking [bg], S. Siddhanta [cy], T. Siemiarczuk [bv], D. Silvermyr [cb], C. Silvestre [bp], G. Simatovic [bh,co], G. Simonetti [ah], R. Singaraju [dt], R. Singh [ch], S. Singha [dt,bx], V. Singhal [dt], B.C. Sinha [dt], T. Sinha [cr], B. Sitar [ak], M. Sitta [ae], T.B. Skaali [v], K. Skjerdal [s], R. Smakal [al], N. Smirnov [dz], R.J.M. Snellings [ax], C. Søgaard [ag], R. Soltz [bt], M. Song [eb], J. Song [cm], C. Soos [ah], F. Soramel [ac], I. Sputowska [dh], M. Spyropoulou-Stassinaki [cf], B.K. Srivastava [cl], J. Stachel [cj], I. Stan [bc], G. Stefanek [bv], M. Steinpreis [t], E. Stenlund [ag], G. Steyn [cg], J.H. Stiller [cj], D. Stocco [dd], M. Stolpovskiy [av], P. Strmen [ak], A.A.P. Suaide [dk], M.A. Subieta Vásquez [y], T. Sugitate [ar], C. Suire [au], R. Sultanov [ay], M. Šumbera [ca], T. Susa [co], T.J.M. Symons [bs], A. Szanto de Toledo [dk], I. Szarka [ak], A. Szczepankiewicz [dh,ah], M. Szymański [dw], J. Takahashi [dl], M.A. Tangaro [af], J.D. Tapia Takaki [au], A. Tarantola Peloni [be], A. Tarazona Martinez [ah], A. Tauro [ah], G. Tejeda Muñoz [c], A. Telesca [ah], A. Ter Minasyan [cq], C. Terrevoli [af], J. Thäder [cn], D. Thomas [ax], R. Tieulent [dm], A.R. Timmins [dn], D. Tlusty [al], A. Toia [an,ac,cw], H. Torii [dq], L. Toscano [cv], V. Trubnikov [d], D. Truesdale [t], W.H. Trzaska [aq], T. Tsuji [dq], A. Tumkin [cp], R. Turrisi [cw], T.S. Tveter [v], J. Ulery [be], K. Ullaland [s], J. Ulrich [bl,bd], A. Uras [dm], G.M. Urciuoli [db], G.L. Usai [x], M. Vajzer [al,ca], M. Vala [bk,az], L. Valencia Palomo [au], P. Vande Vyvre [ah], J.W. Van Hoorne [ah], M. van Leeuwen [ax], L. Vannucci [br], A. Vargas [c], R. Varma [as], M. Vasileiou [cf], A. Vasiliev [cq], V. Vechernin [dv], M. Veldhoen [ax], M. Venaruzzo [w], E. Vercellin [y], S. Vergara [c], R. Vernet [i], M. Verweij [ax], L. Vickovic [df], G. Viesti [ac], J. Viinikainen [aq], Z. Vilakazi [cg], O. Villalobos Baillie [cs], Y. Vinogradov [cp], L. Vinogradov [dv], A. Vinogradov [cq], T. Virgili [ad], Y.P. Viyogi [dt], A. Vodopyanov [bk], M.A. Völkl [cj], S. Voloshin [dx], K. Voloshin [ay], G. Volpe [ah], B. von Haller [ah], I. Vorobyev [dv], D. Vranic [cn,ah], J. Vrláková [am], B. Vulpescu [bo], A. Vyushin [cp], B. Wagner [s], V. Wagner [al], R. Wan [h], Y. Wang [h], M. Wang [h], Y. Wang [cj], K. Watanabe [dr], M. Weber [dn], J.P. Wessels [ah,bg], U. Westerhoff [bg], J. Wiechula [ds], J. Wikne [v], M. Wilde [bg], G. Wilk [bv], M.C.S. Williams [cx], B. Windelband [cj], L. Xaplanteris Karampatsos [di], C.G. Yaldo [dx], Y. Yamaguchi [dq], S. Yang [s], P. Yang [h], H. Yang [o,ax], S. Yasnopolskiy [cq], J. Yi [cm], Z. Yin [h], I.-K. Yoo [cm], J. Yoon [eb], W. Yu [be], X. Yuan [h], I. Yushmanov [cq], V. Zaccolo [by], C. Zach [al], C. Zampolli [cx], S. Zaporozhets [bk], A. Zarochentsev [dv], P. Závada [bb], N. Zaviyalov [cp], H. Zbroszczyk [dw], P. Zelnicek [bd], I.S. Zgura [bc], M. Zhalov [cc], H. Zhang [h], X. Zhang [bs,bo,h], Y. Zhang [h], D. Zhou [h], F. Zhou [h], Y. Zhou [ax], H. Zhu [h], J. Zhu [h], X. Zhu [h], J. Zhu [h], A. Zichichi [ab,m], A. Zimmermann [cj], G. Zinovjev [d], Y. Zoccarato [dm], M. Zynovyev [d], M. Zyzak [be]

[a] *Academy of Scientific Research and Technology (ASRT), Cairo, Egypt*
[b] *A.I. Alikhanyan National Science Laboratory (Yerevan Physics Institute) Foundation, Yerevan, Armenia*
[c] *Benemérita Universidad Autónoma de Puebla, Puebla, Mexico*
[d] *Bogolyubov Institute for Theoretical Physics, Kiev, Ukraine*
[e] *Bose Institute, Department of Physics and Centre for Astroparticle Physics and Space Science (CAPSS), Kolkata, India*
[f] *Budker Institute for Nuclear Physics, Novosibirsk, Russia*
[g] *California Polytechnic State University, San Luis Obispo, CA, United States*
[h] *Central China Normal University, Wuhan, China*
[i] *Centre de Calcul de l'IN2P3, Villeurbanne, France*
[j] *Centro de Aplicaciones Tecnológicas y Desarrollo Nuclear (CEADEN), Havana, Cuba*
[k] *Centro de Investigaciones Energéticas Medioambientales y Tecnológicas (CIEMAT), Madrid, Spain*
[l] *Centro de Investigación y de Estudios Avanzados (CINVESTAV), Mexico City and Mérida, Mexico*
[m] *Centro Fermi – Museo Storico della Fisica e Centro Studi e Ricerche "Enrico Fermi", Rome, Italy*
[n] *Chicago State University, Chicago, United States*
[o] *Commissariat à l'Energie Atomique, IRFU, Saclay, France*
[p] *COMSATS Institute of Information Technology (CIIT), Islamabad, Pakistan*
[q] *Departamento de Física de Partículas and IGFAE, Universidad de Santiago de Compostela, Santiago de Compostela, Spain*
[r] *Department of Physics, Aligarh Muslim University, Aligarh, India*
[s] *Department of Physics and Technology, University of Bergen, Bergen, Norway*
[t] *Department of Physics, Ohio State University, Columbus, OH, United States*
[u] *Department of Physics, Sejong University, Seoul, South Korea*
[v] *Department of Physics, University of Oslo, Oslo, Norway*
[w] *Dipartimento di Fisica dell'Università and Sezione INFN, Trieste, Italy*
[x] *Dipartimento di Fisica dell'Università and Sezione INFN, Cagliari, Italy*
[y] *Dipartimento di Fisica dell'Università and Sezione INFN, Turin, Italy*
[z] *Dipartimento di Fisica dell'Università 'La Sapienza' and Sezione INFN, Rome, Italy*
[aa] *Dipartimento di Fisica e Astronomia dell'Università and Sezione INFN, Catania, Italy*
[ab] *Dipartimento di Fisica e Astronomia dell'Università and Sezione INFN, Bologna, Italy*
[ac] *Dipartimento di Fisica e Astronomia dell'Università and Sezione INFN, Padova, Italy*
[ad] *Dipartimento di Fisica 'E.R. Caianiello' dell'Università and Gruppo Collegato INFN, Salerno, Italy*

[ae] Dipartimento di Scienze e Innovazione Tecnologica dell'Università del Piemonte Orientale and Gruppo Collegato INFN, Alessandria, Italy
[af] Dipartimento Interateneo di Fisica 'M. Merlin' and Sezione INFN, Bari, Italy
[ag] Division of Experimental High Energy Physics, University of Lund, Lund, Sweden
[ah] European Organization for Nuclear Research (CERN), Geneva, Switzerland
[ai] Fachhochschule Köln, Köln, Germany
[aj] Faculty of Engineering, Bergen University College, Bergen, Norway
[ak] Faculty of Mathematics, Physics and Informatics, Comenius University, Bratislava, Slovakia
[al] Faculty of Nuclear Sciences and Physical Engineering, Czech Technical University in Prague, Prague, Czech Republic
[am] Faculty of Science, P.J. Šafárik University, Košice, Slovakia
[an] Frankfurt Institute for Advanced Studies, Johann Wolfgang Goethe-Universität Frankfurt, Frankfurt, Germany
[ao] Gangneung-Wonju National University, Gangneung, South Korea
[ap] Gauhati University, Department of Physics, Guwahati, India
[aq] Helsinki Institute of Physics (HIP) and University of Jyväskylä, Jyväskylä, Finland
[ar] Hiroshima University, Hiroshima, Japan
[as] Indian Institute of Technology Bombay (IIT), Mumbai, India
[at] Indian Institute of Technology Indore, Indore (IITI), India
[au] Institut de Physique Nucléaire d'Orsay (IPNO), Université Paris-Sud, CNRS-IN2P3, Orsay, France
[av] Institute for High Energy Physics, Protvino, Russia
[aw] Institute for Nuclear Research, Academy of Sciences, Moscow, Russia
[ax] Nikhef, National Institute for Subatomic Physics and Institute for Subatomic Physics of Utrecht University, Utrecht, Netherlands
[ay] Institute for Theoretical and Experimental Physics, Moscow, Russia
[az] Institute of Experimental Physics, Slovak Academy of Sciences, Košice, Slovakia
[ba] Institute of Physics, Bhubaneswar, India
[bb] Institute of Physics, Academy of Sciences of the Czech Republic, Prague, Czech Republic
[bc] Institute of Space Sciences (ISS), Bucharest, Romania
[bd] Institut für Informatik, Johann Wolfgang Goethe-Universität Frankfurt, Frankfurt, Germany
[be] Institut für Kernphysik, Johann Wolfgang Goethe-Universität Frankfurt, Frankfurt, Germany
[bf] Institut für Kernphysik, Technische Universität Darmstadt, Darmstadt, Germany
[bg] Institut für Kernphysik, Westfälische Wilhelms-Universität Münster, Münster, Germany
[bh] Instituto de Ciencias Nucleares, Universidad Nacional Autónoma de México, Mexico City, Mexico
[bi] Instituto de Física, Universidad Nacional Autónoma de México, Mexico City, Mexico
[bj] Institut Pluridisciplinaire Hubert Curien (IPHC), Université de Strasbourg, CNRS-IN2P3, Strasbourg, France
[bk] Joint Institute for Nuclear Research (JINR), Dubna, Russia
[bl] Kirchhoff-Institut für Physik, Ruprecht-Karls-Universität Heidelberg, Heidelberg, Germany
[bm] Korea Institute of Science and Technology Information, Daejeon, South Korea
[bn] KTO Karatay University, Konya, Turkey
[bo] Laboratoire de Physique Corpusculaire (LPC), Clermont Université, Université Blaise Pascal, CNRS-IN2P3, Clermont-Ferrand, France
[bp] Laboratoire de Physique Subatomique et de Cosmologie (LPSC), Université Joseph Fourier, CNRS-IN2P3, Institut Polytechnique de Grenoble, Grenoble, France
[bq] Laboratori Nazionali di Frascati, INFN, Frascati, Italy
[br] Laboratori Nazionali di Legnaro, INFN, Legnaro, Italy
[bs] Lawrence Berkeley National Laboratory, Berkeley, CA, United States
[bt] Lawrence Livermore National Laboratory, Livermore, CA, United States
[bu] Moscow Engineering Physics Institute, Moscow, Russia
[bv] National Centre for Nuclear Studies, Warsaw, Poland
[bw] National Institute for Physics and Nuclear Engineering, Bucharest, Romania
[bx] National Institute of Science Education and Research, Bhubaneswar, India
[by] Niels Bohr Institute, University of Copenhagen, Copenhagen, Denmark
[bz] Nikhef, National Institute for Subatomic Physics, Amsterdam, Netherlands
[ca] Nuclear Physics Institute, Academy of Sciences of the Czech Republic, Řež u Prahy, Czech Republic
[cb] Oak Ridge National Laboratory, Oak Ridge, TN, United States
[cc] Petersburg Nuclear Physics Institute, Gatchina, Russia
[cd] Physics Department, Creighton University, Omaha, NE, United States
[ce] Physics Department, Panjab University, Chandigarh, India
[cf] Physics Department, University of Athens, Athens, Greece
[cg] Physics Department, University of Cape Town and iThemba LABS, National Research Foundation, Somerset West, South Africa
[ch] Physics Department, University of Jammu, Jammu, India
[ci] Physics Department, University of Rajasthan, Jaipur, India
[cj] Physikalisches Institut, Ruprecht-Karls-Universität Heidelberg, Heidelberg, Germany
[ck] Politecnico di Torino, Turin, Italy
[cl] Purdue University, West Lafayette, IN, United States
[cm] Pusan National University, Pusan, South Korea
[cn] Research Division and ExtreMe Matter Institute EMMI, GSI Helmholtzzentrum für Schwerionenforschung, Darmstadt, Germany
[co] Rudjer Bošković Institute, Zagreb, Croatia
[cp] Russian Federal Nuclear Center (VNIIEF), Sarov, Russia
[cq] Russian Research Centre Kurchatov Institute, Moscow, Russia
[cr] Saha Institute of Nuclear Physics, Kolkata, India
[cs] School of Physics and Astronomy, University of Birmingham, Birmingham, United Kingdom
[ct] Sección Física, Departamento de Ciencias, Pontificia Universidad Católica del Perú, Lima, Peru
[cu] Sezione INFN, Catania, Italy
[cv] Sezione INFN, Turin, Italy
[cw] Sezione INFN, Padova, Italy
[cx] Sezione INFN, Bologna, Italy
[cy] Sezione INFN, Cagliari, Italy
[cz] Sezione INFN, Trieste, Italy
[da] Sezione INFN, Bari, Italy
[db] Sezione INFN, Rome, Italy
[dc] Nuclear Physics Group, STFC Daresbury Laboratory, Daresbury, United Kingdom
[dd] SUBATECH, Ecole des Mines de Nantes, Université de Nantes, CNRS-IN2P3, Nantes, France
[de] Suranaree University of Technology, Nakhon Ratchasima, Thailand

[df] *Technical University of Split FESB, Split, Croatia*
[dg] *Technische Universität München, Munich, Germany*
[dh] *The Henryk Niewodniczanski Institute of Nuclear Physics, Polish Academy of Sciences, Cracow, Poland*
[di] *The University of Texas at Austin, Physics Department, Austin, TX, United States*
[dj] *Universidad Autónoma de Sinaloa, Culiacán, Mexico*
[dk] *Universidade de São Paulo (USP), São Paulo, Brazil*
[dl] *Universidade Estadual de Campinas (UNICAMP), Campinas, Brazil*
[dm] *Université de Lyon, Université Lyon 1, CNRS/IN2P3, IPN-Lyon, Villeurbanne, France*
[dn] *University of Houston, Houston, TX, United States*
[do] *University of Technology and Austrian Academy of Sciences, Vienna, Austria*
[dp] *University of Tennessee, Knoxville, TN, United States*
[dq] *University of Tokyo, Tokyo, Japan*
[dr] *University of Tsukuba, Tsukuba, Japan*
[ds] *Eberhard Karls Universität Tübingen, Tübingen, Germany*
[dt] *Variable Energy Cyclotron Centre, Kolkata, India*
[du] *Vestfold University College, Tonsberg, Norway*
[dv] *V. Fock Institute for Physics, St. Petersburg State University, St. Petersburg, Russia*
[dw] *Warsaw University of Technology, Warsaw, Poland*
[dx] *Wayne State University, Detroit, MI, United States*
[dy] *Wigner Research Centre for Physics, Hungarian Academy of Sciences, Budapest, Hungary*
[dz] *Yale University, New Haven, CT, United States*
[ea] *Yildiz Technical University, Istanbul, Turkey*
[eb] *Yonsei University, Seoul, South Korea*
[ec] *Zentrum für Technologietransfer und Telekommunikation (ZTT), Fachhochschule Worms, Worms, Germany*

[1] M.V. Lomonosov Moscow State University, D.V. Skobeltsyn Institute of Nuclear Physics, Moscow, Russia.
[2] University of Belgrade, Faculty of Physics and "Vinča" Institute of Nuclear Sciences, Belgrade, Serbia.
[3] Institute of Theoretical Physics, University of Wroclaw, Wroclaw, Poland.